In Situ Heating TEM Study of Onion-like WS_2 and MoS_2 Nanostructures Obtained via MOCVD

Nicole Zink,[†] Helen Annal Therese,[†] Julien Pansiot,[†] Aswani Yella,[†] Florian Banhart,[‡] and Wolfgang Tremel*[,†]

Institut für Anorganizche Chemie and Analytische Chemie, Johannes Gutenberg-Universität Mainz, Duesbergweg 10-14, D-55099 Mainz, Germany, and Institut für Physikalische Chemie, Johannes Gutenberg-Universität Mainz, Welderweg 11, D-55099, Mainz, Germany

Received August 8, 2006. Revised Manuscript Received March 26, 2007

We report on the in situ heating transmission electron microscopy (TEM) study of WS_2 and MoS_2 nanoparticles obtained from metal–organic chemical vapor deposition (MOCVD). The general behavior of MoS_2 and WS_2 is similar: Round, amorphous particles in the pristine sample transform to hollow, onion-like particles upon annealing. A second type of particle with straight layers exhibits only minor changes. A significant difference between both compounds could be demonstrated in their crystallization behavior. The results of the in situ heating experiments are compared to those obtained from an ex situ annealing process under Ar.

Introduction

The synthesis of nanostructures from layered materials such as onion-like particles and nanotubes was first achieved in the carbon system.[1,2] Tenne and co-workers opened up the pathway to another class of compounds, the layered transition metal chalcogenides MQ_2 (M = transition metal; Q = S, Se, Te), that are forming similar morphologies and dubbed them inorganic fullerene-like materials (IF).[3–6] Various synthesis techniques for these IFs have been established so far, among them oxide to sulfide conversion,[7–11] decomposition of suitable precursors,[12–15] transport reactions,[16–18] laser ablation,[19–21] arc discharge, template methods,[8] microwave synthesis,[22,23] and chemical vapor deposition (CVD).[24]

Except for the oxide to sulfide conversion, which has been scrutinized,[25,26] the growth mechanism of such nanostructures is still subject to discussion. Understanding the principles of the growth mechanism will facilitate to tailor the chemical synthesis according to specific needs concerning compound, size, morphology, etc. In situ heating transmission electron microscopy is a powerful method to monitor structural changes,[27–31] nucleation processes,[32] and phase evolutions[21,33,34] during the process itself. In this contribution we will employ this technique to evaluate the growth mechanism of MS_2 (M = Mo, W) nanoparticles synthesized via the metal–organic chemical vapor deposition (MOCVD) method.

* Corresponding author: Fax (+49) 6131-39-25605, Tel (+49) 6131-39-25135, e-mail tremel@mail.uni-mainz.de.
[†] Institut für Anorganizche Chemie and Analytische Chemie.
[‡] Institut für Physikalische Chemie.

(1) Kroto, H. W.; Heath, J. R.; O'Brien, S. C.; Curl, R. F.; Smalley, R. E. *Nature (London)* **1985**, *318*, 162.
(2) Iijima, S. *Nature (London)* **1991**, *354*, 56.
(3) Tenne, R.; Margulis, L.; Genut, M.; Hodes, G. *Nature (London)* **1992**, *360*, 444.
(4) Tenne, R.; Margulis, L.; Hodes, G. *Adv. Mater.* **1993**, *5*, 386.
(5) Homyonfer, M.; Mastai, Y.; Hershfinkel, M.; Volterra, V.; Hutchison, J. L.; Tenne, R. *J. Am. Chem. Soc.* **1996**, *118*, 7804.
(6) Tenne, R.; Margulis, L.; Feldman, Y.; Homyonfer, M. *Mater. Res. Soc. Symp. Proc.* **1995**, *359*, 111.
(7) Rothschild, A.; Tenne, R.; Sloan, J.; York, A. P. E.; Green, M. L. H.; Sloan, J.; Hutchison, J. L. *Chem. Commun.* **1999**, 363.
(8) Whitby, R. L. D.; Hsu, W. K.; Lee, T. H.; Boothroyd, C. B.; Kroto, H. W.; Walton, D. R. M. *Chem. Phys. Lett.* **2002**, *359*, 68.
(9) Hsu, W. K.; Zhu, Y. Q.; Yao, N.; Firth, S.; Clark, R. J. H.; Kroto, H. W.; Walton, D. R. M. *Adv. Funct. Mater.* **2001**, *11*, 69.
(10) (a) Therese, H. A.; Li, J. X.; Kolb, U.; Tremel, W. *Solid State Sci.* **2005**, *7*, 67. (b) Therese, H. A.; Zink, N.; Kolb, U.; Tremel, W. *Solid State Sci.* **2006**, *8*, 1133.
(11) Li, X. L.; Li, Y. D. *Chem.—Eur. J.* **2003**, *9*, 2726.
(12) Nath, M.; Govindaraj, A.; Rao, C. N. R. *Adv. Mater.* **2001**, *13*, 283.
(13) Nath, M.; Rao, C. N. R. *Chem. Commun.* **2001**, 2236.
(14) Zelenski, C. M.; Dorhout, P. K. *J. Am. Chem. Soc.* **1998**, *120*, 734.
(15) Chen, J.; Li, S.-L.; Gao, F.; Tao, Zh.-L *Chem. Mater.* **2003**, *15*, 1012.
(16) Zhu, Y. Q.; Hsu, W. K.; Terrones, H.; Grobert, N.; Chang, B. H.; Terrones, M.; Wei, B. Q.; Kroto, H. W.; Walton, D. R. M.; Boothroyd, C. B.; Kinloch, I.; Chen, G. Z.; Windle, A. H.; Fray, D. J. *J. Mater. Chem.* **2000**, *10*, 2570.
(17) Remskar, M.; Mrzel, A.; Skraba, Z.; Jesih, A.; Demsar, J.; Stadelman, P.; Levy, F.; Mihailovic, D. *Science* **2001**, *292*, 479.
(18) Remskar, M.; Mrzel, A.; Sanjines, R.; Cohen, H.; Levy, F. *Adv. Mater.* **2003**, *15*, 237.
(19) Nath, M.; Rao, C. N. R.; Popovitz-Biro, R.; Albu-Yaron, A.; Tenne, R. *Chem. Mater.* **2004**, *16*, 2238.
(20) Sen, R.; Govindaraj, A.; Suenaga, K.; Suzuki, S.; Kataura, H.; Iijima, S.; Achiba, Y. *Chem. Phys. Lett.* **2001**, *340*, 242.
(21) Schuffenhauer, C.; Parkinson, B. A.; Jin-Phillipp, N. Y.; Joly-Pottuz, L.; Martin, J.-M.; Popovitz-Biro, R.; Tenne, R. *Small* **2005**, *1*, 1100.
(22) Vollath, D.; Szabo, D. V. *Mater. Lett.* **1998**, *35*, 236.
(23) Vollath, D.; Szabo, D. V. *Acta Mater.* **2000**, *48*, 953.
(24) Etzkorn, J.; Therese, H. A.; Rocker, F.; Zink, N.; Kolb, U.; Tremel, W. *Adv. Mater.* **2005**, *17*, 2372.
(25) Tenne, R.; Homyonfer, M.; Feldman, Y. *Chem. Mater.* **1998**, *10*, 3225.
(26) Tenne, R. *Chem.—Eur. J.* **2002**, *8*, 5297.
(27) Lee, H. J.; Ni, H.; Wu, D. T.; Ramirez, A. G. *Mater. Trans.* **2006**, *47*, 527.
(28) Hu, P. A.; Liu, Y. Q.; Fu, L.; Cao, L. C.; Zhu, D. B. *Appl. Phys. A: Mater. Sci. Process.* **2005**, *80*, 1413.
(29) Agrawal, A.; Cizeron, J.; Colvin, V. L. *Microsc. Microanal.* **1998**, *4*, 269.
(30) Rankin, J. *J. Am. Ceram. Soc.* **1999**, *82*, 1560.
(31) Rankin, J.; Sheldon, B. W. *Mater. Sci. Eng., A* **1995**, *204*, 48.
(32) Hidaka, K.; Tanikoshi, S.; Nishi, K.; Aono, Y. *Mater. Trans., JIM* **1995**, *36*, 251.
(33) Chatterjee, K.; Howe, J. M.; Johnson, W. C.; Murayama, M. *Acta Mater.* **2004**, *52*, 2923.
(34) Ballif, C.; Regula, M.; Remskar, M.; Sanjines, R.; Levy, F. *Surf. Sci.* **1996**, *366*, L703.

10.1021/cm061867k CCC: $40.75
Published on Web 12/11/2007

Recently, the synthesis of inorganic fullerene-like MoS_2, $MoSe_2$, and WS_2 particles with the aid of the MOCVD method was reported.[24,35] The results of a two-step and a single-step reaction process were compared.[35] The two-step synthesis consisted of the MOCVD process of primary nanoparticles followed by an annealing in inert atmosphere in a conventional tube furnace. For the single-step process the MOCVD synthesis was carried out at higher temperatures without isolating the intermediate product. Depending whether a two-step or a single-step process was used, the main product consisted of hollow or filled onion-like structures, respectively. The MOCVD synthesis alone resulted in the formation of two types of nanoparticle intermediates: (i) small, irregular shaped particles (S-type) and (ii) bigger, round particles (R-type). Annealing in argon led to two types of product nanoparticles: (i) needle-like, well-crystallized (N-type) and (ii) hollow onion-like particles (O-type).

The parameter fields (e.g., temperature within the MOCVD reactor, heating/cooling rates, gas flow, annealing time, annealing temperature, etc.) are large; thus, the set of parameters for optimum synthesis conditions is difficult to screen experimentally. The resemblance in morphology of round (R) and hollow onion-like (O) particles on the one hand and small, straight layered (S) and needle-like (N) particles on the other lent support to the hypothesis that R- and O-type, as well as S- and N-type particles, respectively, are in some way related to each other. If S- and R-type particles were intermediates in the formation of N- and O-particles, an optimization should mainly concern the first MOCVD reaction step. Otherwise, the influence of reaction parameters of the annealing process such as temperature, time, and gas flow should be more thoroughly examined.

To understand the transformation of S- and R-type particles upon annealing, we followed their structural evolution by in situ heating in a transmission electron microscope (TEM) in order to extract information about the growth mechanism of inorganic fullerene-like particles (by real-space imaging) as well as their ordering and crystallinity (by electron diffraction).

Experimental Section

The experiment requires two steps: (i) the synthesis of MS_2 (M = Mo, W) nanoparticles material and (ii) the subsequent annealing within a transmission electron microscope.

MOCVD Synthesis. Reactants ($M(CO)_6$ (M = Mo, W) and S) are heated with the aid of heating tapes in the left and right arms of a T-shaped quartz reactor setup. An Ar flow transports the reactants to the reaction zone which is located in the coil of an induction furnace. A schematic representation of the experimental setup for this first step and a more detailed description of the experimental conditions was given by Etzkorn et al.[24] The MS_2 (M = M, W) samples obtained in this first reaction step are labeled MOCVD product in the sequel; T_{ind} corresponds to the reaction temperature of the MOCVD experiment, i.e., the temperature of the induction coil. T_{anneal} and t_{anneal} are the annealing temperature [°C] and annealing time [h] of the subsequent annealing step under Ar.

(35) Zink, N.; Pansiot, J.; Kieffer, J.; Therese, H. A.; Panthöfer, M.; Rocker, F.; Kolb, U.; Tremel, W. *Chem. Mater.* **2008**, in press.

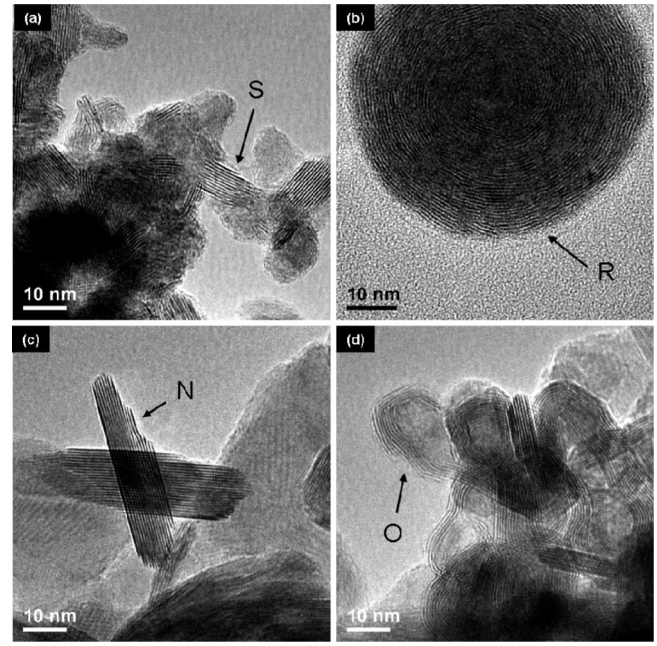

Figure 1. HRTEM images of (a) small particles (S) with straight layers and (b) round particles (R) in a pristine WS_2 (750) sample and of (c) needle-like (N) and (d) onion-like (O) particles in an annealed WS_2 (450/800-1) sample. Note: R-type particles (b) in low-temperature (450 °C) syntheses are similar in morphology but do not exhibit layer fringes.

The nomenclature used for the products in this paper is as follow: The pristine product before the annealing step contains nanowhisker-type small particles (S) with straight layers and spherical particles (R/round). After the annealing needle-like (N) particles and onion-like (O) particles are obtained. The temperature of the reactor during the synthesis is written in parentheses (e.g., WS_2 (450)); the temperature of the annealing step is given as the second number in parentheses (e.g., WS_2 (450/800)).

In Situ Heating TEM Study. For this second step, samples synthesized at 450 °C were deposited on a Cu grid coated with a holey amorphous carbon film (Plano, S147-3) from an ethanolic suspension. The grids were placed in a single tilt heating stage (GATAN). To minimize thermal drift, a water cooling of the outer part of the sample holder was installed.

Before heating, the sample was screened for suitable particles and their positions were registered. Image recording was started only after temperature constancy/stability throughout the sample had been achieved. The sample was subsequently analyzed at 200, 250, 300, 350, 400, 450, 500, 600, 700, and 800 °C for the WS_2 and 100, 300, 500, 600, 700, and 750 °C for the MoS_2 samples.

Instrumental Details. Transmission electron microscopy (TEM) was performed on a Philips CM12 instrument at an acceleration voltage of 120 kV. High-resolution and in situ heating studies were carried out on a FEI TECNAI F30 ST microscope (300 kV acceleration voltage, field emission gun). Fourier filtering was employed for noise-reduction in some of the images. An example of the procedure is given in the Supporting Information.

Results and Discussion

Pristine Sample at the Example of WS_2. Figure 1a,b shows the pristine WS_2 particles, (i) small, irregular shaped particles (S-type) and (ii) bigger, round particles (R-type) that were obtained from the MOCVD process at 750 °C before the annealing step. Figure 1c,d displays the samples displayed in Figure 1a,b after annealing. Figure 1c shows

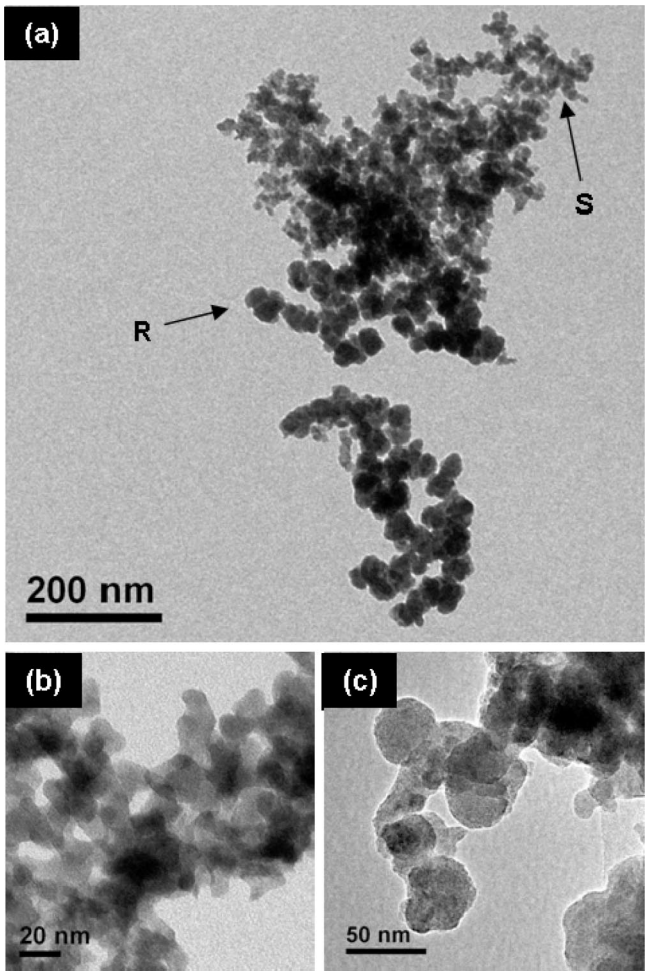

Figure 2. TEM image of a WS_2 (450) sample (a) before annealing. (b) and (c) show TEM micrographs of S-type (b) and R-type (c) particles at higher resolution.

needle-like, well-crystallized (N-type) and Figure 1d hollow onion-like particles (O-type) particles after annealing under argon.

Figure 2 displays an overview TEM image of a WS_2 (450) sample *before annealing*. The pristine material consists of a network-like agglomerate of nanoparticles. Two distinct types of particles can be observed: smaller irregular shaped particles (named S-type hereafter) and bigger round particles (R-type). High-resolution pictures of a typical S- and R-type particle are shown in parts b and c of Figure 2, respectively.

In Situ Heating TEM Study. In the following section, the results of the in situ heating TEM studies are presented, first for WS_2 and then for MoS_2.

Tungsten Disulfide. In Figure 3 a high-resolution (HR) TEM image of a R-type particle heated to 250 °C is shown. The following discussion is based on the evolution of three marked areas (white rectangles) upon annealing. Figure 4 represents Fourier filtered HRTEM images of the central part of the R-type particle. At 250 °C, layer formation in the central part can already be observed. This contradicts a strict outward-in growing process as might have been expected. The inner part is more or less an isotropic amorphous mixture. Therefore, no preferred orientation of the layers, e.g., to avoid dangling bonds,

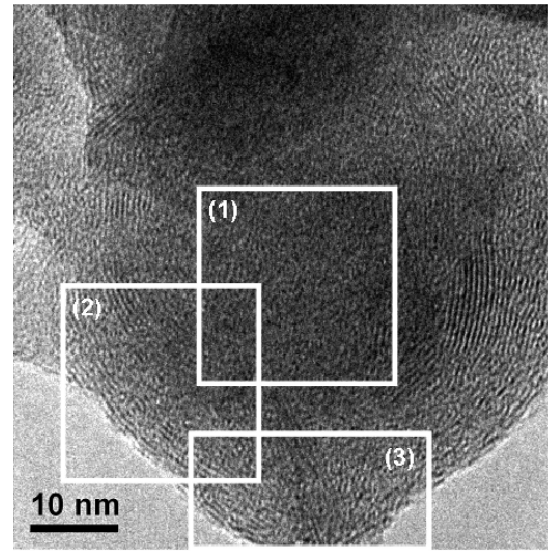

Figure 3. HRTEM picture of an R-type particle at 250 °C. The structural transformation within three marked areas (white rectangles) is monitored in the sequel.

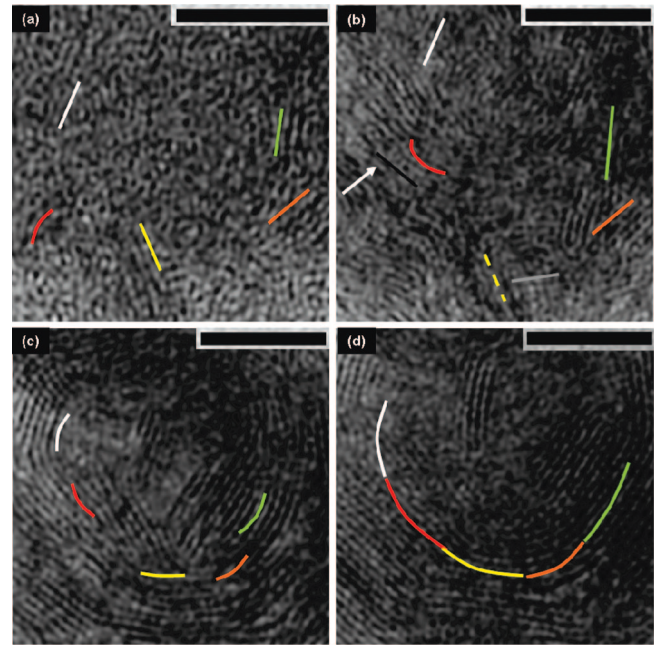

Figure 4. Evolution in the central part (area 1 in Figure 3) of R-type particles monitored by means of IFFT of HRTEM images upon annealing at 250 (a), 400 (b), 600 (c), and 800 °C (d). Colored lines mark areas with WS_2 layers. The center remains filled throughout the heating. Scale bar = 10 nm.

should be observed. This is indeed the case, as can be seen from the arbitrary orientation of the colored lines (representing a parallel package of layers) in Figure 4a. At 400 °C (b) the orientation of the red line has turned about 90°. This reorientation may be triggered by in coming outer layer front (black line), thus leading to the observed rearrangement of the inner layers (red line).

This process of reorientation in favor of tangential layers can also be observed considering as an example the yellow line in Figure 4b. At 600 °C (Figure 4c) a tangential orientation of the layer packages emerges. The size of layers has increased in both directions and an incipient bending of

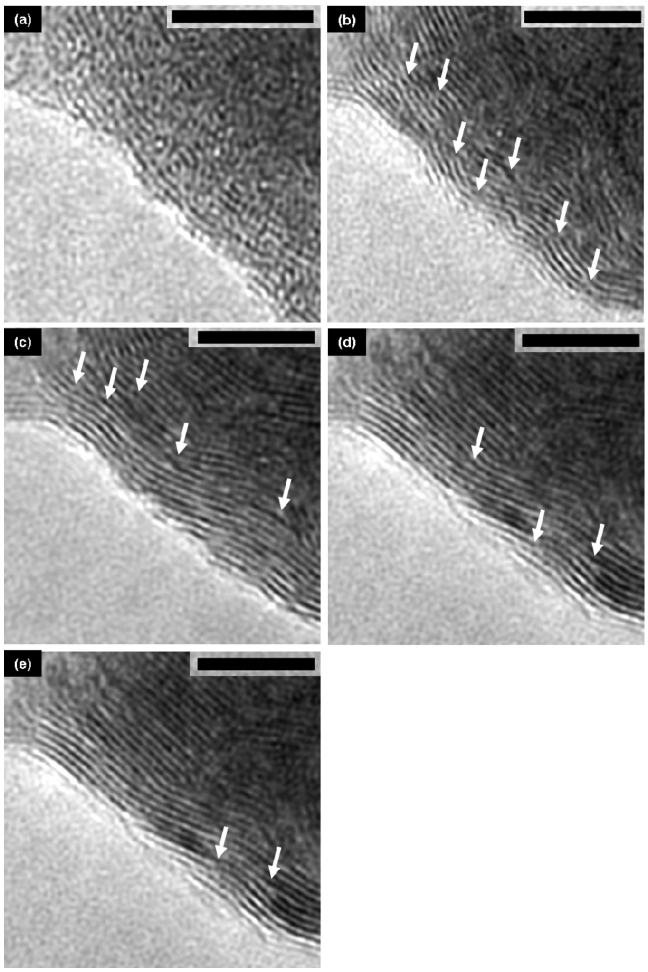

Figure 5. IFFT of HRTEM images of an area at the particle boundary (area 2 in Figure 3) at 250 (a), 400 (b), 600 (c), 700 (d), and 800 °C (e). Some defects are marked with white arrows. Scale bar = 10 nm.

the layers is observed. At 800 °C (Figure 4d) adjacent layer packages are joined at their edges, enclosing one-half of the particle center. Only a few defects remain.

In the second area (Figure 5), the layer formation at the particle boundary can be studied. Between 250 (a) and 400 °C (b) WS_2 layers are formed tangentially to the outer boundary. Along the layer numerous defects can be observed (arrows). Note that stacking faults between layers do not abound. At higher temperatures, first the defects in the outer layers start healing (c) followed by those in the more central portion of the particle, according to a defect annealing kind of process.

Two processes can be observed in the third area (Figure 6.) WS_2 layers that are stacked along the radial direction exhibit unsaturated bonds at the outer surface ("dangling bonds").[36–38] This is energetically not favorable. Therefore,

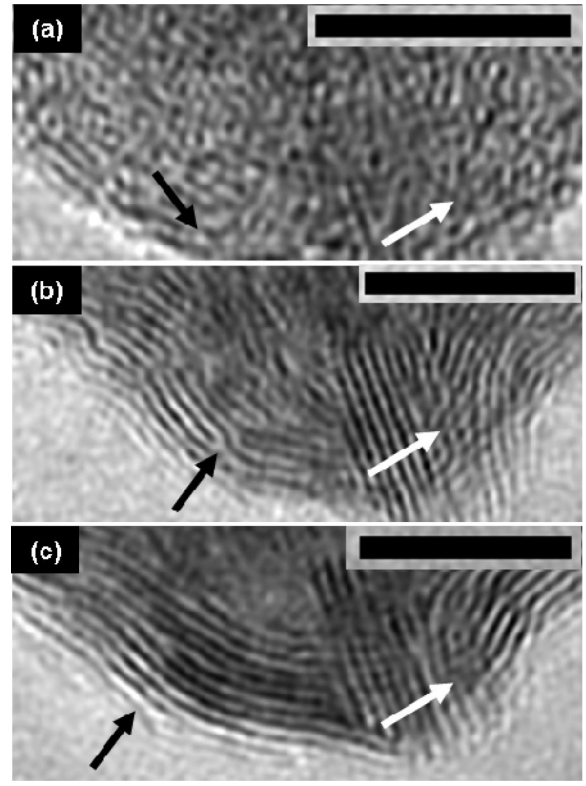

Figure 6. IFFT of HRTEM images of an R-type particle heated at 250 (a), 400 (b), and 800 °C (c). Successive healing of defects and transformation of radial to tangential layers are indicated with black and white arrows, respectively. Scale bar = 10 nm.

a transformation to the thermodynamically more stable arrangement of tangential layers occurs at higher temperatures (see white arrows Figure 6a–c).

Upon annealing the simultaneous formation and growth of WS_2 layers at different positions becomes evident. Interconnection of two layer packages leads to defects resembling edge dislocations that are subsequently healed upon annealing (see black arrows in Figure 6a–c).

d_{002} values as obtained from FFT analyses of the in situ heating TEM images are well above the value $d_{calc} = 0.616$ nm for the bulk material. This can be attributed to a large number of defects, e.g., interstitial atoms between the layers.

In conclusion, annealing of spherical amorphous WS_2 particles leads first to the nucleation of several crystallites which coalesce upon sustained annealing at higher temperatures. Grains whose basal planes are parallel to the surface of the particles are preferred since surface dangling bonds can be prevented. Hence, an energetically favorable structure with spherically closed concentric layers is formed (see Figure 7).

Small straight-layered (S) particles, which are already crystalline before annealing, become nearly defect-free when heated to 250 °C (Figure 8a). Further annealing does not lead to a significant increase in layer size or number of layers or to the formation of anisotropic, needle-like structures (N-type) as observed in annealed samples. At some positions, a bending of layer packages can be observed at higher temperatures (Figure 8b).

A possible explanation for the lack of layer growth as compared to the round (R) particles might be related to the

(36) Cox, P. A. *The Electronic Structure and Chemistry of Solids*; Oxford Science Publications: Oxford, 1987.
(37) (a) Tremel, W. *Angew. Chem., Int. Ed.* **1999**, *38*, 2175. (b) Tenne, R. *Angew. Chem., Int. Ed.* **2003**, *42*, 5124.
(38) (a) Leist, A.; Stauf, S.; Löken, S.; Finckh, E. W.; Lüdtke, S.; Unger, K. K.; Assenmacher, W.; Mader, W.; Tremel, W. *J. Mater. Chem* **1998**, *8*, 241. (b) Berntsen, N.; Gutjahr, T.; Loeffler, L.; Gomm, J. R.; Seshadri, R.; Tremel, W. *Chem. Mater.* **2003**, *15*, 4498.

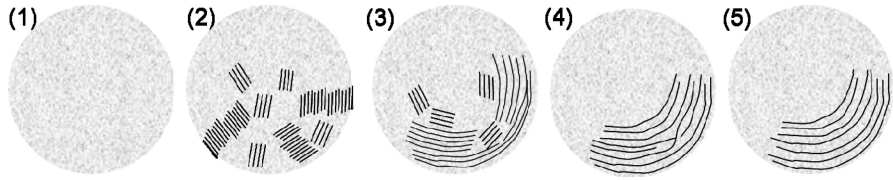

Figure 7. Schematic growth mechanism for R-type particles in a WS_2 sample: (1) amorphous material, (2) incipient layer formation, (3) preferred formation of closed shells at the boundary with basal layers parallel to the surface, (4) movement of defects to the outside, (5) formation of closed shells. Layers are only shown for part of the particle.

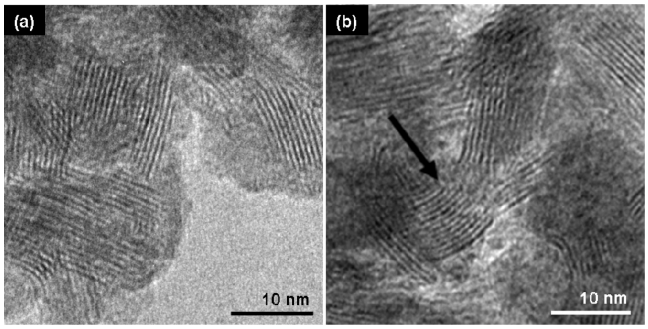

Figure 8. HRTEM images of S-type WS_2 particles at 250 (a) and 800 °C (b). Bending of layers is indicated with a black arrow.

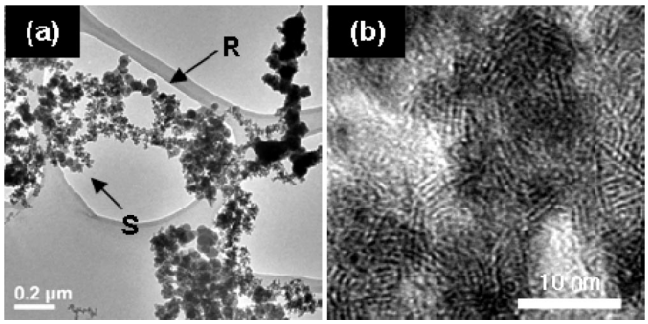

Figure 9. TEM overview (a) and HRTEM of S-type particles in a MoS_2 sample before annealing. Refer to text for definition of S- and R-type particles marked with arrows in (a).

different nature of the original amorphous material for S- and R-type particles. In R-type particles a stoichiometric mixture of W:S = 1:2 is achieved, whereas in S-type particles tungsten is prevailing as was shown by energy dispersive X-ray analyses. We assume that during the heating process polynuclear metal clusters are formed by decarbonylation. Eventually this process leads to the formation of W clusters or nanoparticles.

$$2W(CO)_6 \xrightarrow{\Delta T} W_2(CO)_{10} + 2CO \xrightarrow{\Delta T} \ldots \xrightarrow{\Delta T} W_n \qquad (1)$$

In the reaction zone of the MOCVD setup, sulfur from the gas phase will react with a part of this amorphous W material resulting in the formation of amorphous S-type WS_2 particles. The amount of sulfur that diffuses into these W-clusters is limited, and therefore only nanosized particles can be formed. The vacuum in TEM prevents the delivery of more sulfur from other parts of the sample to the S-type particles. Therefore, the heating leads only to an increase in crystallinity but not in the size of the particles. In contrast, when the sample is annealed under Ar, sulfur from sulfur-rich parts of the sample can be transported to the S-type WS_2 particles where it reacts with the outermost layer of still unreacted

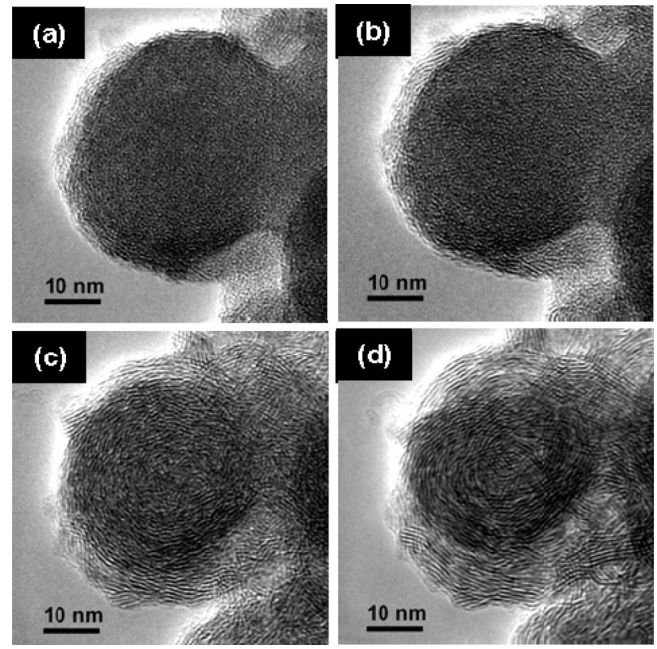

Figure 10. TEM image of an R-type particle in a MoS_2 sample at 24 (a), 100 (b), 300 (c), and 500 °C (d).

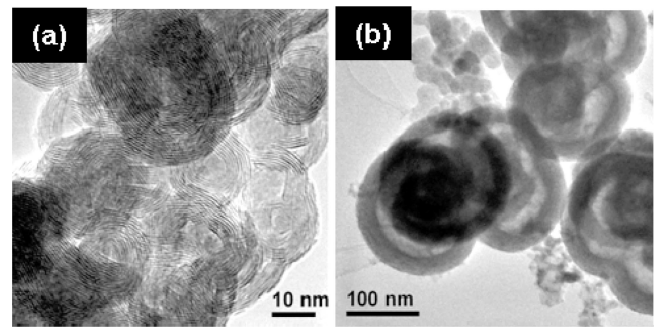

Figure 11. TEM images at 700 °C of hollow onions in a MoS_2 sample. Note the significantly larger hollow core for bigger particles (b) as compared to particles of half the size (a).

amorphous W to complete the formation of WS_2. It is likely that the formation of new WS_2 is more favorable at the edges of the WS_2 sheets (where unsaturated metal atoms are present). This leads to anisotropic particle growth perpendicular to the stacking direction *c*. It remains unclear why needles and not slabs are formed, as *a* and *b* directions are crystallographically equivalent. A preferred growth in only one of these directions is difficult to rationalize.

One possible explanation might be the presence of WO_x impurities (with adsorbed water or air as oxygen source) as a reaction intermediate as WO_x is known to exhibit needle-like morphology, and a subsequent resulfurization is responsible for this peculiar behavior.[10,25,26]

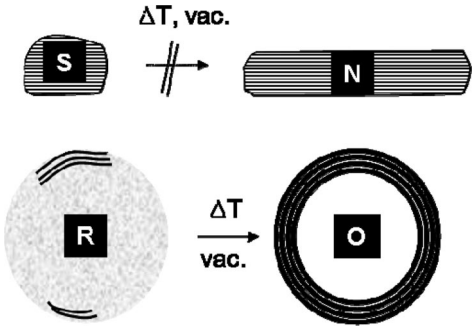

Figure 12. Schematic representation of monitored particle development during in situ heating TEM study. Refer to text for particles type (S, N, R, O) definition.

The amorphous R-type particle on the other hand should consist of an intimate mixture of W and S on an atomic scale. The presence of both W and S is confirmed by EDX analyses in a 1:1.5–1:2 ratio. The amount of S as a much lighter material than W might be underestimated by EDX semi-quantitative analysis. The spherical morphology of R-type particles could hint to the growth from a liquid sulfur droplet into which W is diffused.

Molybdenum Disulfide. In the following section, the results for in situ heating experiments of MoS_2 obtained from a MOCVD synthesis at 450 °C will be discussed.

The R-type particles are amorphous. In some of them, small layer fragments ($d_{002} = 0.645$ nm) in the outer region can be observed already at room temperature. At 100 °C more layered material is formed at the particle boundaries and primarily tangential to them. At 300 °C layer fragments can be seen throughout the particle; i.e., the major portion of the amorphous material has transformed to MoS_2.

The newly formed layers exhibit a vast number of defects. Upon further annealing a defect annealing takes place in both, the central and outer parts of the particles, leading to increased crystallinity. Simultaneously, a transformation from nontangential to tangential layers is observed. Bending of layers starts as early as at 500 °C.

At about 700–750 °C, the continued healing of defects and the bending of layers leads to the formation of onion-like particles with a hollow core (Figure 11). A large variation is observed for the corresponding d_{002} values. Among the variety of R-type particles, two extremes can be distinguished according to their size: (i) particles with diameters of 50 nm and less (majority, Figure 11a) and those with diameters of 100 nm and more (only few examples, Figure 11b). Surprisingly, the larger particles do not contain significantly more outer layers (30–50 layers) than the smaller ones (10–30 layers) but rather have a distinctly larger hollow core compared to the smaller ones. Two explanations for the occurrence of the restricted number of layers are feasible: (i) material depletion, i.e., no amorphous "material" that could crystallize is available anymore, or (ii) the time/temperature of reaction was not sufficient to complete the reaction. As in samples heated for 12 h (and more) under Ar at 800 °C no filled onion-like structures could be observed even for large particles, we think that a "shortage" of material is responsible for the formation of hollow nanoparticles with a restricted number of layers. A similar phenomenon was observed in the formation of hollow calcium carbonate particles and was attributed to densification upon crystallization of amorphous calcium carbonate along with an outward-in growing mechanism.[39]

S-type particles show only a minor growth upon annealing. A minor part of the primary particles showed a resemblance in their outer morphologies to S-type particles, although only very few or no (002)-layer fringes were observed. A more detailed analysis revealed weak lattice fringes with $d = 0.224 \pm 0.046$ nm, which corresponds to either elemental Mo ($d_{110} = 0.223$ nm) or 2H-MoS_2 ($d_{103} = 0.228$ nm). Upon annealing, a "halo" of lighter contrast appeared, and the formation of very few (002) lattice fringes was noticed at the boundaries. In EDX analyses, Mo, C, O, and Cu (due to the grid) could clearly be identified. Because of the overlap of the S(K)- and Mo(L)-signals, the Mo/S ratio could not be evaluated. Nevertheless, the results peak fitting with and without S point toward the absence of S in these. Thus, we think that this part of the sample can be attributed to Mo clusters in analogy to the results presented above for the formation of WS_2.

Comparison between IF-WS_2 and IF-MoS_2. In this last section we compare the results for tungsten and molybdenum sulfide. In both compounds the crystallization of the pristine sample, consisting of two types of particles (small, straight-layered (S) and round (R)), starts upon annealing with more or less randomly orientated layers. To minimize the amount of unsaturated bonds at the MS_2-layer edges (2-fold coordination instead of 3-fold for S, 4-fold coordination instead of 6-fold for the transition metal[38]), a transformation of layers arranged in a random or nontangential orientation into tangential layers in the R-type particles takes place. The large number of defects (e.g., edge dislocation) observed in the primary particles is reduced considerably upon annealing. Hollow onion-like particles are formed in this step. Annealing has no considerable effect on the S-type particles except for healing of the small amount of defects and a slight increase in size. This was attributed to sulfur deficiency in the metal clusters (M = Mo, W) formed in the initial phase of the synthesis by the thermal decarbonylation of the metal–carbonyl precursors.

Despite the similarities in the general morphology of WS_2 and MoS_2 and their behavior upon annealing some noteworthy differences are observed: (i) The formation of the R-type particles for MoS_2 starts already in the pristine samples. (ii) The nucleation and growth, i.e., the formation of layers of ordered "crystalline" from amorphous material (although defects are still present), is completed at lower temperatures (<300 °C) for MoS_2 compared to WS_2 (400–500 °C). (iii) The crystallization process seems different: For MoS_2, the layer formation starts throughout the R-type particle, and the layers are already tangentially aligned. Above 300 °C, the healing of defects is the predominant process. In contrast, for WS_2, the crystallization starts at the outer particle boundaries (although some arbitrarily oriented layer fragments are also present in the central portion of the particles). An outside-in growing process of the tangentially oriented

(39) Loges, N.; Graf, K.; Nasdala, L.; Tremel, W. *Langmuir* **2006**, *22*, 3073.

outer layers finally leads to a reorientation of the central layer fragments. This development takes place over a wide temperature range (300–800 °C) in contrast to the very fast process in MoS_2. (iv) The overall W:S (or Mo:S) ratio is in the particles is 1:2. The S-type particles are typically slightly more tungsten (molybdenum)-rich than the R-type particles. Increasing the reaction temperature leads to a depletion of the sulfur content, especially for the R-type particles, as predicted by thermodynamics. In summary, we conclude that the formation of IF-MoS_2 proceeds more smoothly than that of IF-WS_2. This may be attributed to stronger metal–metal bonding for W as compared to Mo, hampering the reaction with sulfur.

Comparison to the ex Situ Annealed Sample. The present TEM in situ heating study establishes a link between the morphologies of MoS_2 and WS_2 nanoparticles obtained by MOCVD before and after annealing under Ar, i.e., between S- and N-type particles on the one hand and R- and O-type particles on the other. For both compounds MoS_2 and WS_2, a transformation of R-type particles into hollow onions (similar to O-type particles obtained from ex situ annealing experiments) could be demonstrated.[36] The crystallinity of the ex situ samples is slightly higher than that of the in situ samples. This can be attributed to enhanced surface diffusion (and therefore more facile particle growth) in the surrounding Ar gas atmosphere compared to an dynamic vacuum in a transmission electron microscope, where no surface diffusion is possible.

An (anisotropic) growth of S-type particles into needle-like (N-type) structures could not be observed. We therefore believe that surface diffusion (i.e., presence of gas phase) plays a substantial role in the formation of N-type particles.

Nevertheless, the present study shows that the amount of the desired hollow onion-like structures originates from R-type particles present in the pristine sample. Screening of optimized parameters for a preferable pure O-type sample should therefore essentially be limited to the reaction parameters of the MOCVD setup (such as reaction temperature and time, gas flow, choice of precursors, geometry of the glass setup, etc.).

Conclusion

To summarize, the in situ heating TEM study of MoS_2 and WS_2 nanoparticles obtained via MOCVD allowed us to monitor the growth mechanism of hollow onion-like nanoparticles in which defect annealing processes play a major role. A relationship between particles of the pristine sample with a round morphology (R-type) and the resulting hollow onion-like particles (O) could be established (Figure 12). Therefore, an optimization of the synthesis of such hollow fullerene-like structures should primarily concern the optimization of the MOCVD process in order to obtain only R-type particles in the first reaction step that can be converted to IF-MQ_2 (M = Mo, W) by subsequent annealing. S-type particles did not grow into needles upon in situ annealing. Although the morphologies of the pristine particles (MoS_2/WS_2) obtained during the first step of the synthesis of are similar, the layer formation in the MoS_2 primary particles proceeds more smoothly than that for WS_2.

Acknowledgment. This research was supported by the Deutsche Forschungsgemeinschaft (DFG). J. Pansiot and A. Yella are recipients of an Erasmus fellowship of the European Community and a fellowship from the graduate school of excellence of the state of Rhineland-Palatinate, respectively.

Supporting Information Available: HRTEM, corresponding FFT, and resulting IFFT. This material is available free of charge via the Internet at http://pubs.acs.org.

CM061867K